JOURNAL OF GUIDANCE, CONTROL, AND DYNAMICS
Vol. 32, No. 4, July–August 2009

Simulating Active Vibration Attenuation in Underactuated Spatial Structures

S. Woods* and W. Szyszkowski†
University of Saskatchewan, Saskatoon, Saskatchewan, S7N 5A9, Canada

DOI: 10.2514/1.41219

The active optimal attenuation of vibrations in spatial structures, modeled by finite elements with a possibly large number of degrees of freedom, is considered. The problem is formulated as underactuated in modal space, such that the desired number of controlled modes may be greater than the number of independent discrete actuators. Consequently, modal variables are coupled via second-order nonholonomic constraints that impose limitations on the dynamically admissible trajectories that a given structure may undergo. The optimality equations for the problem with a quadratic performance index are derived in a compact form involving time derivatives of all modal variables and Lagrange multipliers, which are required to ensure that the constraints are satisfied. These equations are solved by applying symbolic differential operators. The procedure employs standard finite element and symbolic mathematical software to render the optimal actuation forces and trajectories of all controlled modes (or any selected degrees of freedom) to attenuate vibrations. For illustration the method, referred to as the constrained modal space optimal control, is used to synthesize the active controls and predict response of a mast structure.

I. Introduction

THE numerical simulation of active vibration attenuation in continuous structures is normally an underactuated control problem because there are theoretically an infinite number of degrees of freedom (DOF) to be controlled (attenuated) by a typically small number of discrete actuators [1]. Modelling these structures with finite elements (FE) reduces the number of DOF to a finite, but often large, number of DOF. In the *direct dynamics*, where a system's response is sought for given applied forces, underactuated and fully actuated systems are handled routinely by the standard methods of computational mechanics. However, in active vibration attenuation, a number of actuation forces applied to maneuver all DOF in a desired trajectory are to be determined constituting the *inverse dynamics* problem. For fully actuated systems, inverse dynamics usually requires a less challenging direct "inversion" of independent control forces into the same number of independent (uncoupled) DOF. For underactuated systems, the inverse dynamics is more challenging because the actuation forces have to be inverted into the DOF that are coupled by nonholonomic constraints (involving DOF accelerations), posing limitations on the set of *admissible* DOF trajectories. Therefore, *any* arbitrarily selected desired trajectory may not be admissible, complicating the synthesis of the forces to control it.

The vibrating motion of most mechanical systems can conveniently be approximated using the superposition of a relatively small number of their most significant modes that transform the set of infinite or finite but large DOF into a handful of generalized modal variables [2]. This is helpful for many practical applications, in which the number of vibration modes needed to accurately (depending on application) model the system dynamics is small enough that an equal number of discrete actuators may be applied to control them. Thus, the problem becomes fully actuated in modal space, and any requested modal variable trajectories are admissible because all modal variables are independent. This approach, widely documented in literature, is called independent modal space control (IMSC) because each modal variable is directly related to a corresponding independent modal control [3]. Clearly, the IMSC approach cannot be applied to underactuated systems, that is, when the number of modes is greater than the number of actuators.

For such systems the so-called constrained modal space optimal control (CMSOC) approach was proposed in [4], and further detailed in [5]. This approach permits the simulation of active attenuation of underactuated linear systems and ensures that all considered system trajectories are admissible (i.e., satisfy the nonholonomic constraints coupling generalized modal variables). The CMSOC method formulates underactuated systems by adding a sufficient number of "dummy" actuators, alongside the "real" actuators, to create an artificially "augmented" fully actuated system. The zero-force dummy actuators are used to generate the algebraic constraints in terms of the modal controls and to define the coefficients of the so-called normalized matrix of constraints. In terms of modal variables, these constraints become differential (nonholonomic) and are satisfied with the help of time-varying Lagrange multipliers (which in turn secures the dynamic admissibility of any resulting trajectories).

Pontryagin's principle is used to formulate the optimal control problem in the form of a two-point-boundary-value problem involving a set of coupled differential equations to be solved in terms of all modal variables and Lagrange multipliers. These equations, though of high order, are solved efficiently with the use of symbolic operators and a symbolic math computer program. The procedure, when combined with an FE structural code, is capable of simulating the entire active vibration attenuation problem for a wide variety of elastic structures. This permits the inspection and evaluation of the effectiveness, or controllability, of particular configurations of the actuators.

This paper presents the CMSOC method in application to attenuating the vibrations in a spatial mast structure that is subjected to an initial disturbance. Several different positions and numbers of actuators will be investigated, in search of "good" configurations for eliminating vibrations. Such configurations should be characterized by fast attenuation rates and low input actuators forces requirements.

II. Problem Formulation

The equations of motion for an elastic structure are written as follows:

$$\mathbf{M}\ddot{\mathbf{q}} + \mathbf{C}\dot{\mathbf{q}} + \mathbf{K}\mathbf{q} = \mathbf{B}\mathbf{F} \tag{1}$$

Presented as Paper 6076 at the 12th AIAA/ISSMO Multidisciplinary Analysis and Optimization Conference, Victoria, BC, Canada, 10–12 August 2008; received 24 September 2008; revision received 12 January 2009; accepted for publication 20 January 2009.

*M.Sc. Student, Department of Mechanical Engineering.
†Professor, Department of Mechanical Engineering.

Vector $\mathbf{q}$ contains n_m components representing the system DOF, whereas $\mathbf{M}$, $\mathbf{C}$, and $\mathbf{K}$ are constant mass, damping, and stiffness matrices (of size $n_m \times n_m$), respectively. The augmented force vector $\mathbf{F}$, of size n_m, contains n_a real actuation forces forming the subvector vector $\mathbf{F_a}$ and $n_d = n_m - n_a$ dummy forces contained in the subvector $\mathbf{F_d}$, such that $\mathbf{F} = [\mathbf{F_a}^T \quad \mathbf{F_d}^T]^T$. Square matrix $\mathbf{B}$ ($n_m \times n_m$) assigns the vector $\mathbf{F}$ to the DOF.

The task in active vibration attenuation is to maneuver a disturbed elastic structure to rest, which is described by the following boundary conditions:

$$\mathbf{q}(0) = \mathbf{q_0} \qquad \dot{\mathbf{q}}(0) = \dot{\mathbf{q}}_\mathbf{0} \qquad \mathbf{q}(t_f) = \mathbf{0} \qquad \dot{\mathbf{q}}(t_f) = \mathbf{0} \tag{2}$$

where $\mathbf{q_0}$ and $\dot{\mathbf{q}}_\mathbf{0}$ are vectors representing the initial position and velocity (at time $t = 0s$) of the DOF, respectively. At time t_f, which may be infinite for time-invariant problems, the structure reaches a state of rest.

A. Dynamics of Underactuated Elastic Structures in Modal Space

The set of equations within Eq. (1) are uncoupled when mapped into modal space, where the vector of DOF $\mathbf{q}$ (size n_m) is transformed to the equal sized vector of modal variables $\eta = [\eta_1 \quad \cdots \quad \eta_{n_m}]^T$. Similarly, force vector $\mathbf{F}$ is related to an equal-sized vector of modal controls $\mathbf{U} = [u_1 \quad \cdots \quad u_{n_m}]^T$. These transformations take the following forms:

$$\mathbf{q} = \Phi\eta \tag{3a}$$

$$\mathbf{U} = (\Phi^T\mathbf{B})\mathbf{F} = \hat{\mathbf{B}}\mathbf{F} \tag{3b}$$

where $\hat{\mathbf{B}} = \Phi^T\mathbf{B}$ is the transfer matrix between vectors $\mathbf{F}$ and $\mathbf{U}$. Mode shape matrix $\Phi = [\phi_1 \quad \cdots \quad \phi_{n_m}]$, consisting of n_m mode shape vectors ϕ_i, provides the mapping between vectors $\mathbf{q}$ and η and satisfies the following orthogonality conditions:

$$\Phi^T\mathbf{M}\Phi = \mathbf{I} \tag{4a}$$

$$\Phi^T\mathbf{K}\Phi = \Omega \tag{4b}$$

where $\mathbf{I}$ is the unitary matrix and Ω is the diagonal matrix of ordered frequencies with the terms $\Omega_{ii} = \omega_i^2$. Each mode shape vector ϕ_i and frequency ω_i are solutions to the eigenvalues problem $(\mathbf{K} - \omega_i^2\mathbf{M})\phi_i = 0$, for $i = 1, \ldots, n_m$.

By applying the transformations in Eqs. (3a) and (3b) and orthogonality conditions in Eqs. (4a) and (4b), the set of equations within Eq. (1) is uncoupled in modal space, yielding

$$\mathbf{I}\,\ddot{\eta} + \Delta\dot{\eta} + \Omega\eta = \mathbf{U} \tag{5}$$

where diagonal matrix Δ has the terms $\Delta_{ii} = 2\zeta_i\omega_i$ with modal natural damping ratios $\zeta_i = \phi_i^T\mathbf{C}\phi_i$.

In standard computational mechanics, the direct dynamics are required to obtain a system's response to applied forces, whereby $\mathbf{U}$ is determined directly from Eq. (3b), modal variable responses are obtained through Eq. (5), and then DOF responses are obtained through Eq. (3a). In active vibration attenuation, the inverse dynamics are required to obtain the attenuating forces. *First*, modal control vector $\mathbf{U}$ is determined from Eq. (5) and *then* the real actuation forces are obtained through the inverse of Eq. (3b).

The dummy, or zero-force, actuator(s) contained in vector $\mathbf{F_d}$ were added to ensure the existence of matrix $\hat{\mathbf{B}}^{-1}$, required in the inverse of Eq. (3b). Once computed, $\hat{\mathbf{B}}^{-1}$ may be partitioned to better distinguish between those elements contributing to the mapping of real actuation forces and those elements mapping the dummy actuation forces, whose actions are reduced to zero (i.e., $\mathbf{F_d} = [0 \quad \cdots \quad 0]^T$) to render a set of constraints. Thus the operation takes the following form:

$$\hat{\mathbf{B}}^{-1}\mathbf{U} = \mathbf{F} \Rightarrow \begin{bmatrix} \tilde{\mathbf{B}}_\mathbf{a} & \tilde{\mathbf{B}}_\mathbf{r} \\ \mathbf{A_a} & \mathbf{A_r} \end{bmatrix} \begin{bmatrix} \mathbf{U_a} \\ \mathbf{U_r} \end{bmatrix} = \begin{bmatrix} \mathbf{F_a} \\ \mathbf{F_d} \end{bmatrix} \tag{6}$$

Square submatrix $\tilde{\mathbf{B}}_\mathbf{a}$ is of size $n_a \times n_a$ and square submatrix $\mathbf{A_r}$ is of size $n_d \times n_d$. For mathematical convenience, vector $\mathbf{U}$ is divided into two subvectors $\mathbf{U_a} = [u_1 \ldots u_{n_a}]^T$ and $\mathbf{U_r} = [u_{n_a+1} \cdots u_{n_m}]^T$, referred to as *essential* and *redundant* modal controls vectors, respectively. To be consistent with this naming convention, the modal variables vector may be similarly partitioned such that vector $\eta_\mathbf{a} = [\eta_1 \cdots \eta_{n_a}]^T$ contains essential modal variables and $\eta_\mathbf{r} = [\eta_{n_a+1} \cdots \eta_{n_m}]^T$ contains redundant modal variables.

Given the null-valued dummy force vector $\mathbf{F_d}$ (size $n_d \times 1$) the bottom n_d rows of Eq. (6) (bottom partitions) define constraints on the system in the following form:

$$\mathbf{A}_\mathbf{a}\mathbf{U_a} + \mathbf{A_r}\mathbf{U_r} = \mathbf{0} \tag{7}$$

Matrix $\mathbf{A} = [\mathbf{A_a} \quad \mathbf{A_r}]$ of size $n_d \times n_m$, to be referred to as the matrix of constraints, may contain $n_d n_m$ nonzero coefficients A_{ij}. However, when normalized such that $A_{ii} = 1$, $A_{k,i} = 0$ for $k > i$ (left bottom corner), and $A_{k,n_a+1+k} = 0$ for $1 \le k \le n_d - 1$ (right upper corner), the matrix of constraints take a form that is independent of the locations of dummy actuators, written as follows:

$$\mathbf{A} = \left[\begin{array}{ccccccccccc} 1 & A_{12} & A_{13} & \cdots & A_{1,n_d} & \cdots & A_{1,n_a} & A_{1,n_a+1} & & & \\ & 1 & A_{23} & \cdots & A_{2,n_d} & \cdots & A_{2,n_a} & A_{2,n_a+1} & A_{2,n_a+2} & & \\ & & 1 & \cdots & \cdots & \cdots & \cdots & \cdots & \cdots & & \\ & & & \cdots & \cdots & \cdots & \cdots & \cdots & \cdots & \cdots & \\ & & & & 1 & \cdots & A_{n_d,n_a} & A_{n_d,n_a+1} & A_{n_d,n_a+2} & \cdots & A_{n_d,n_m} \end{array}\right] \tag{8}$$

As it will be shown, this normalized form gives some indications on the capacity for certain configurations of real actuators to attenuate each modal variable defining the system.

The real actuation force(s) may be computed from the top partitions of Eq. (6) in terms of all modal controls, but they can also be obtained solely in terms of essential modal controls vector $\mathbf{U_a}$ by applying n_d constraints in the form of Eq. (7) to eliminate redundant modal controls vector $\mathbf{U_r}$. Thus, n_a active attenuating forces contained in vector $\mathbf{F_a}$ can be obtained in terms of n_a essential modal controls in vector $\mathbf{U_a}$ from the following operation:

$$\mathbf{F}_\mathbf{a} = (\tilde{\mathbf{B}}_\mathbf{a} - \tilde{\mathbf{B}}_\mathbf{r}\mathbf{A_r}^{-1}\mathbf{A_a})\mathbf{U_a} = \bar{\mathbf{B}}\mathbf{U_a} \tag{9}$$

Square matrix $\bar{\mathbf{B}} = \tilde{\mathbf{B}}_\mathbf{a} - \tilde{\mathbf{B}}_\mathbf{r}\mathbf{A_r}^{-1}\mathbf{A_a}$ ($n_a \times n_a$), referred to as the pseudotransfer matrix, relates essential modal controls to real actuator forces. Equation (9) requires the nonsingularity of matrix $\mathbf{A_r}$; otherwise it cannot be used to determine the redundant controls in terms of the independent controls. Likewise, the pseudotransfer matrix $\bar{\mathbf{B}}$, also independent of the choice of dummy actuators, must be nonsingular.

The respective forms of matrices $\mathbf{A_r}$ and $\bar{\mathbf{B}}$ indicate characteristics of a particular actively controlled structure. The following two scalar measures λ and κ referred to as the *rate* and *effort* parameters, are adopted to reflect control performance (or the effectiveness of certain actuators' locations):

$$\lambda = |\det \mathbf{A_r}| \tag{10a}$$

$$\kappa = |\det \bar{\mathbf{B}}| \tag{10b}$$

These parameters can be used only to compare the effectiveness of different configurations of actuators for a particular mechanical system. Matrix $\mathbf{A_r}$ contains the last n_d columns of the normalized matrix $\mathbf{A}$ in Eq. (8), and so it is always triangular (thus $\det \mathbf{A_r} = A_{1,n_a+1} \times A_{2,n_a+2} \times \cdots \times A_{n_d,n_m}$). Ideally, the best rate of attenuation is achieved for all modal variables if all nonzero elements of matrix $\mathbf{A_r}$ have a value of unity, resulting in the rate parameter $\lambda = |\det \mathbf{A_r}| = 1$. This is due to the fact that for such actuator locations, the redundant modal controls will have similar magnitudes

as the essential modal controls. Consequently, redundant modal variables will be attenuated at a similar rate as the independent modal variables, which in turn are attenuated according to the IMSC scheme.

On the other hand, the effort parameter κ from Eq. (10b) will generally indicate actuator configurations that have small maximum force requirements by producing a small scalar value. This is because the independent modal controls are determined first irrespective of actuators positioning and next mapped into the actuation forces.

B. Optimal Attenuation of Underactuated Elastic Structures

The *optimal* attenuation for an active structure minimizes a performance index in the form

$$J = \frac{1}{2}\int_0^{t_f} ((\eta^T \hat{\mathbf{Q}}_\mathbf{d}\eta) + (\dot{\eta}^T \hat{\mathbf{Q}}_\mathbf{v}\dot{\eta}) + (\mathbf{U}^T \hat{\mathbf{R}}\mathbf{U}))\mathrm{d}t \to \min \qquad (11)$$

where matrices $\hat{\mathbf{Q}}_\mathbf{d}$, $\hat{\mathbf{Q}}_\mathbf{v}$, and $\hat{\mathbf{R}}$, with the diagonal terms $\hat{Q}_{dii}$, $\hat{Q}_{vii}$, and $\hat{R}_{ii}$ $(i = 1, \ldots, n_m)$, weight the bracketed terms that, in turn, represent a system's potential energy, kinetic energy, and actuator work. The attenuation interval t_f may be chosen arbitrarily, or its value can be determined through optimization by adding an additional constant weighting term in the integrand of Eq. (11). Otherwise the attenuation interval may be considered infinite for time-invariant problems ($t_f \to \infty$), which are of significant interest for simulating structures attenuated in a closed-loop control schemes. The optimal solution for η (and $\mathbf{U}$) should minimize J in Eq. (11), while satisfying the uncoupled system Eq. (5) and, for underactuated systems, the constraints in the form of Eq. (7) that couple modal variables and modal controls. The set of optimality conditions are obtained by applying the Pontryagin principle [6], for which the Hamiltonian H is defined as follows:

$$H = -\frac{1}{2}(\eta^T \hat{\mathbf{Q}}_\mathbf{d}\eta + \dot{\eta}^T \hat{\mathbf{Q}}_\mathbf{v}\dot{\eta} + \mathbf{U}^T \hat{\mathbf{R}}\mathbf{U}) + \mathbf{P_d}\dot{\eta} + \mathbf{P_v} \times (-\Delta\dot{\eta} - \Omega\eta + \mathbf{U}) + \nu^T \mathbf{A}\mathbf{U} \qquad (12)$$

where $\mathbf{P_d}$ and $\mathbf{P_v}$ are standard costate vectors driving modal variables position and velocity states (η and $\dot{\eta}$) related to Eq. (5). For underactuated systems vector $\mathbf{v} = [\,\upsilon_1 \quad \ldots \quad \upsilon_{n_r}\,]^T$ represents a set of time-dependent Lagrange multipliers applied to enforce the constraints. According to the Pontryagin principle, costate equations take the form

$$\dot{\mathbf{P}}_\mathbf{d} = -\frac{\partial H}{\partial \eta} = \hat{\mathbf{Q}}_\mathbf{d}\eta + \Omega\mathbf{P_v} \qquad (13a)$$

$$\dot{\mathbf{P}}_\mathbf{v} = -\frac{\partial H}{\partial \dot{\eta}} = \hat{\mathbf{Q}}_\mathbf{v}\dot{\eta} - \mathbf{P_d} + \Delta\mathbf{P_v} \qquad (13b)$$

The Hamiltonian is stationary with respect to modal controls if

$$\frac{\partial H}{\partial \mathbf{U}} = -\hat{\mathbf{R}}\mathbf{U} + \mathbf{P_v} + \mathbf{A}^T\mathbf{v} = \mathbf{0} \qquad (14)$$

Substituting Eq. (5) into Eq. (14) gives

$$\mathbf{P_v} = \hat{\mathbf{R}}(\mathbf{I}\ddot{\eta} + \Delta\dot{\eta} + \Omega\eta) - \mathbf{A}^T\mathbf{v} \qquad (15)$$

Substituting Eq. (15) into Eq. (13b) yields

$$\mathbf{P_d} = \hat{\mathbf{Q}}_\mathbf{v}\dot{\eta} - \hat{\mathbf{R}}(\mathbf{I}\dddot{\eta} + \Delta\ddot{\eta} + \Omega\dot{\eta}) + \Delta\hat{\mathbf{R}}(\mathbf{I}\ddot{\eta} + \Delta\dot{\eta} + \Omega\eta) + \mathbf{A}^T\dot{\mathbf{v}} - \Delta\mathbf{A}^T\mathbf{v} \qquad (16)$$

Finally, substituting Eq. (16) into Eq. (13a) generates the set of optimality conditions

$$\hat{\mathbf{R}}\,\dddot{\eta} + (2\Omega\hat{\mathbf{R}} - \hat{\mathbf{Q}}_\mathbf{v} - \hat{\mathbf{R}}\Delta^2)\ddot{\eta} + (\hat{\mathbf{R}}\Omega^2 + \hat{\mathbf{Q}}_\mathbf{d})\eta - (\mathbf{A}^T\ddot{\mathbf{v}} - \Delta\mathbf{A}^T\dot{\mathbf{v}} + \Omega\mathbf{A}^T\mathbf{v}) = \mathbf{0} \qquad (17)$$

For fully-actuated problems, the last term (i.e., $\mathbf{A}^T\ddot{\mathbf{v}} - \Delta\mathbf{A}^T\dot{\mathbf{v}} + \Omega\mathbf{A}^T\mathbf{v}$) in Eq. (17) vanishes because there are no constraints or Lagrange multipliers needed to enforce them. Therefore, a fully actuated problem involves only n_m optimality equations to be solved in terms of n_m uncoupled modal variables in vector η.

For underactuated problems, the set of n_m optimality Eq. (17) contain n_m unknown variables in vector η and n_d unknown components in vector ν. Therefore, these optimality equations must be complemented by the set of n_d constraint equations in Eq. (7) written in terms of η. Substituting $\mathbf{U}$ from the equations within Eq. (5) into Eq. (7) gives the differential form of these constraints as

$$\mathbf{A}\,(\mathbf{I}\ddot{\eta} + \Delta\dot{\eta} + \Omega\eta) = \mathbf{0} \qquad (18)$$

The $n_m + n_d$ Eqs. (17) and (18) are equal in number to the unknown functions contained in vectors η and ν. However, a solution without the participation of boundary conditions is trivial ($\eta = \mathbf{0}$, $\nu = \mathbf{0}$). Therefore, one differential equation in the set of Eqs. (17) and (18) will be considered redundant as it will later be replaced by the set of boundary conditions, and the particular equation to be eliminated is arbitrary.

Boundary conditions shown in Eq. (2) are mapped into modal space by the relation $\eta = \phi^T\mathbf{M}\mathbf{q}$, obtained by inverting Eq. (3a) and applying the orthogonality condition in Eq. (4a), thus rendering

$$\eta(0) = \phi^T\mathbf{M}\mathbf{q_0} \qquad \dot{\eta}(0) = \phi^T\mathbf{M}\dot{\mathbf{q}}_\mathbf{0} \qquad \eta(t_f) = \phi^T\mathbf{M}\mathbf{q_f} \qquad \dot{\eta}(t_f) = \phi^T\mathbf{M}\dot{\mathbf{q}}_\mathbf{f} \qquad (19)$$

The solution to the combined set of Eqs. (17–19) can efficiently be obtained using symbolic differential operator $D^n = \frac{\mathrm{d}^n}{\mathrm{d}t^n}$. Substituting this operator into Eqs. (17) and (18) and subsequently rewriting them in a compact matrix notation gives

$$\begin{bmatrix} \mathbf{E} & -\hat{\mathbf{E}}^T \\ \tilde{\mathbf{E}} & \mathbf{0} \end{bmatrix}\begin{bmatrix} \eta \\ \nu \end{bmatrix} = \mathbf{0} \quad \text{or} \quad \mathbf{E_p}\mathbf{Y} = \mathbf{0} \qquad (20)$$

where

$$\mathbf{E} = \hat{\mathbf{R}}D^4 + (2\hat{\mathbf{R}}\Omega - \hat{\mathbf{Q}}_\mathbf{v} - \hat{\mathbf{R}}\Delta^2)D^2 + (\hat{\mathbf{R}}\Omega^\mathbf{2} + \hat{\mathbf{Q}}_\mathbf{d})$$

$$\hat{\mathbf{E}} = \mathbf{A}(\mathbf{I}D^2 + \Delta D + \Omega), \quad \text{and} \quad \tilde{\mathbf{E}} = \mathbf{A}(\mathbf{I}D^2 - \Delta D + \Omega)$$

Matrix $\mathbf{E_p}$ contains submatrices $\mathbf{E}$, $\tilde{\mathbf{E}}$, and $\hat{\mathbf{E}}$, defined previously. Vector $\mathbf{Y} = [\,\eta^T \quad \nu^T\,]^T$ contains all unknown modal variables and Lagrange multipliers. Note that for fully actuated problems, matrix $\mathbf{E_p}$ in Eq. (20) consists only of submatrix $\mathbf{E}$ and also vector $\mathbf{Y} = \eta^T$ contains no Lagrange multipliers.

The solution to a system described by Eq. (20) involves the roots r_i $(i = 1, \ldots, 4n_m)$ of the following characteristic equation [7], where operator D is replaced by the auxiliary variable r:

$$\det \mathbf{E_P}|_{D\to r} = 0 \qquad (21)$$

The preceding operation always generates a $4n_m^{\text{th}}$ order polynomial with $4n_m$ roots in the form

$$r_i = \pm\alpha_k \pm i\beta_k \qquad (k = 1, \ldots, n_m \quad \text{and} \quad i = 1, \ldots, 4n_m) \qquad (22)$$

The positive real numbers α_k and β_k characterize the response of the kth mode of motion. For nonzero, unique roots in the form of Eq. (22), solution vector $\mathbf{Y}$ consists of $n_m + n_d$ components Y_j that can be written in terms of $4n_m$ independent functions as follows:

$$Y_j = \sum_{k=1}^{n_m}[e^{\alpha_k t}(c_{kj}^1 \sin(\beta_k t) + c_{kj}^2 \cos(\beta_k t)) + e^{-\alpha_k t}(c_{kj}^3 \sin(\beta_k t) + c_{kj}^4 \cos(\beta_k t))] \qquad (23)$$

where $j = 1, \ldots, n_m + n_d$. There are $4n_m(n_m + n_d)$ unknown integration constants $c_{kj}^1, \ldots, c_{kj}^4$ contained in the Eq. (23). Their values are obtained by Eq. (23) into Eqs. (17) and (18) (note that $\mathbf{Y} = [\,\eta_1 \ldots \eta_{n_m} \quad \nu_1 \ldots \nu_{n_d}\,]^T$) and using the method of undetermined coefficients to generate $n_m + n_d$ sets of $4n_m$ linear algebraic equations from which these constants can be solved [7]. Recall that

one scalar differential equation in matrix Eqs. (17) and (18), producing $4n_m$ algebraic equations using the method of undetermined coefficients is redundant and should be replaced by the set of $4n_m$ boundary conditions shown in Eq. (19), to solve for the unknown set of integration constants. All these symbolic operations, including the determination of the roots in the form of Eq. (22) and constants in Eq. (23), may be performed automatically using the MAPLE mathematical program.

For closed-loop control, asymptotically convergent solution functions are required so that vibrations are attenuated over an infinite period of time ($t_f \to \infty$). Hence, the number of integration constants is reduced by half, as terms in Eq. (23) involving positive exponential $e^{\alpha_k t}$ disappear (i.e., $c^1_{kj} = c^2_{kj} = 0$). In the examples to follow, the performance of closed-loop control schemes will be evaluated by comparing their effective settling times $t_i^{3\%}$, defined as the time needed for the ith variable to be reduced to 3% of its initial value, which requires that $\alpha_i t_i^{3\%} \geq 3.5$.

C. Solution Procedure

The solution procedure consists of three phases: a structural FE phase, a control phase, and a verification phase. First, the *structural phase* consists of building an FE model (the ANSYS program was used) and doing a modal analysis to provide the spectrum of frequencies and their mode shapes. For any assumed actuators setup, shown in Eqs. (3–10), in Sec. II.A, may be obtained in this phase. Conveniently, controllability related parameters λ and κ are also obtained in this phase, and so deficiencies in assumed actuator configurations may be detected early on, before the more computationally challenging later phases are attempted.

Next, the *control phase* incorporates the results from the structural phase to formulate and solve Eqs. (17) and (18), defining the optimal attenuation for an underactuated active structure. The attenuation of a known initial disturbance in the form of Eq. (19) is obtained by Eqs. (20–23) via the MAPLE program. This phase renders the optimal forces for each actuator, the expected dynamic responses of the structure, and, for time-invariant problems, the gains for closed-loop control.

The final *verification phase* takes the optimal forces from the control phase and applies them back to the FE model in a direct transient dynamic analysis to verify whether or not the structure's response closely matches that obtained in the control phase. Because the transient analysis may include a larger number of vibration modes (up to n modes), any spillover effects of modes higher than n_m can be detected [8]. These three phases of the procedure allow the entire optimal vibrations control problem to be simulated and "virtually" investigated.

When simulating a fully-actuated control system ($n_m = n_a$ and $n_d = 0$), the CMSOC procedure converges to the IMSC scheme [4], where each mode is controlled independently because there are no constraints in the form of Eq. (7) that couple the motion of modal variables.

In the simulation example to follow, the structural phase and control phase are both addressed but the verification phase has been excluded. Emphasis is given to the understanding of how changing actuator configurations may impact the vibration attenuation performance of the active structure. Therefore, issues such as sensor placements and the corresponding gains of closed-loop systems are omitted.

III. Example: Active Attenuation of Vibrations in a Spatial Mast Structure

The mast structure model, shown in Fig. 1a, mimics the geometry and characteristics of an experimental active structure that was discussed in [9]. The structure extends into the z-direction 1.82 m, with 12 repeating bays (and two irregular half-bays at the clamped end and free end), each 14 cm high. A 1.5 cm thick, circular steel plate is supported at the free end. When viewed along the z direction, the three vertical (parallel to z axis) members form the points of an isosceles triangle with a base of 14 cm and a height 10 cm. The connective joints at the intersection of each 4 mm-diameter member are considered rigid and all material properties are assumed to be typical of industrial-grade steel ($E = 200$ GPa, $\rho = 7800$ kg/m^3). The members near the base of the structure, darkened and labeled with uppercase letters ***A*** through ***E***in Fig. 1, indicate the locations that will be considered for the placement of linear actuators. Point p, at the center of the circular plate supported at the free end, will be used as a location for observing (and plotting) response trajectories.

The first three dominant mode shapes of the mast structure are shown in Figs. 1b–1d, each in isometric views and top-down views (in the negative z direction). In the first vibration mode the mast undergoes flexural bending that approximately occurs in the xz plane at a frequency of $\omega_1 = 8.787$ Hz $= 55.21$ rad/s (i.e., a vibration period of $T_1 = 0.1138$ s). In the second mode similar bending deflections occur, however, they effectively occur in the yz plane and at a slightly higher frequency of $\omega_2 = 10.62$ Hz $= 66.71$ rad/s ($T_2 = 0.09419$ s). In its third mode, the mast approximately twists about an axis parallel to the z axis, through point p, and oscillating at a frequency of $\omega_3 = 67.75$ Hz $= 425.7$ rad/s ($T_3 = 0.01476$ s).

In [9], several feedback algorithms were investigated and experimentally tested on the experimental active structure, which were capable of attenuating the motion of the first two bending modes ($n_m = 2$) using the two actuators ($n_a = 2$) located in positions ***A*** and ***B*** (see Fig. 1). In application, the experimental structure applied piezoelectric linear actuators with collocated force transducers to actively attenuate disturbances based on various feedback control laws. Conveniently, the stiffness and length of the actuators were nearly identical to the steel bars they replaced such that the stiffness of the structure remained unchanged. However, the study was limited to fully actuated ($n_m = n_a$) attenuation schemes, where no more than two modes were considered in dynamics modeling.

Alternatively, the CMSOC method may be applied to design the active attenuation for this same active mast structure, particularly for underactuated setups. The effect of actuator location, number of actuators, and the number of significant modes involved in dynamics modeling, on optimal attenuation forces and simulated responses will be studied. To emphasize the *active* damping, all *passive* damping mechanisms, such as internal and external friction, are neglected.

The location of active members significantly impacts the attenuation performance of the system. Good actuator locations have reasonable authority over the vibration mode shapes they intend to eliminate. Therefore, if an actuator is substituted for a structural element that contains a large fraction of the total modal strain energy in a particular mode shape, then good attenuation of that mode should be expected [9]. For evaluation purposes, the fraction of strain energy for the active member positions ***A***, ***B***, and ***C*** are listed in Table 1 for the first three vibration modes.

Table 1 suggests that substituting an actuator for member ***A*** should results in excellent control of mode 2, whereas substituting for member ***B*** should give excellent control of mode 1, because they each have a large fraction (greater than 10%) of the strain energy associated with these modes. However, these actuators' authority over the third mode should be much worse.

The following cases will be investigated using the CMSOC approach:

1) *Two* actuators, replacing members ***A*** and ***B***, are controlling *two* modes.

2) *One* actuator, replacing member ***A***, is controlling *two* modes.

3) *Two* actuators, replacing members ***A*** and***B***, are controlling *three* modes.

4) *One* actuator, replacing member ***A***, is controlling *three* modes.

In each case, the mast's dynamics (forces, trajectories, etc.) are examined for an assumed initial disturbance of $\eta_1|_{t=0} = \eta_2|_{t=0} = 0.004$, $\eta_3|_{t=0} = 0.001$, and $\dot{\eta}_i|_{t=0} = 0$ ($i = 1, 2, 3$). In the original spatial coordinates, this assumed disturbance causes point p (center of mast's top plate, see Fig. 1) to be deflected 2.28 mm in the x direction, 2.58 mm in the y direction, and rotate counterclockwise 0.548 deg about the z axis.

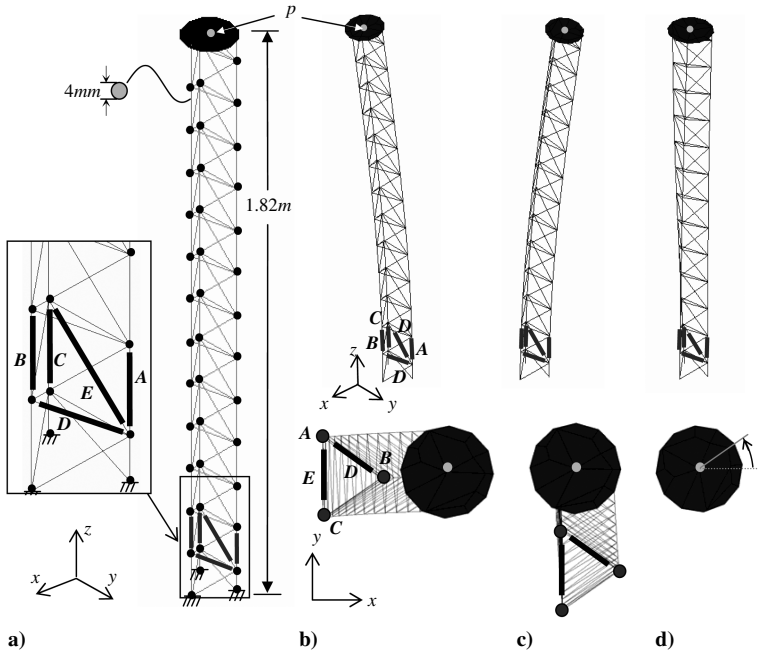

Fig. 1 Diagram showing a) the mast model and its mode shapes for b) the first mode, c) the second mode, and d) the third mode.

The task is to maneuver the structure from this disturbed state to its undeformed resting state. In each case, the time-invariant ($t_f \to \infty$) attenuation that minimizes Eq. (11), with weighting parameters $\hat{\mathbf{Q}}_\mathbf{d} = \Omega$, $\hat{\mathbf{Q}}_\mathbf{v} = \mathbf{I}$, and $\hat{\mathbf{R}} = 0.1\Omega^{-1}$, is sought. Note that in cases 1 and 2, only two modes are considered in the dynamics modeling, hence disturbances causing mast twisting (third mode of vibration) are left unattenuated.

A. Two Actuators, Replacing Members *A* and *B*, Controlling Two Modes

Two actuators placed in the locations of members ***A*** and ***B*** (see Fig. 1) are used to attenuate the first two vibration modes with corresponding forces F_A and F_B ($n_a = n_m = 2$, $n_d = 0$). Because this case is fully actuated, the no constraint Eq. (18), is required, as all trajectories are admissible, and thus no Lagrange multipliers are needed in the optimality Eq. (17). Consequently, only boundary conditions in the form of Eq. (19) are required to obtain the optimal attenuation forces and response trajectories.

The mapping between real actuation forces F_A and F_B and the two modal controls u_1 and u_2, does not require any partitioning as shown in Eq. (6) because, as a fully actuated system, all modal controls are essential (i.e., $\hat{\mathbf{B}}^{-1} = \tilde{\mathbf{B}}_\mathbf{a} = \bar{\mathbf{B}}$). Therefore this mapping takes the following form (results from the ANSYS FE program were used to obtain the terms in matrix $\hat{\mathbf{B}}$):

$$\hat{\mathbf{B}}^{-1}\mathbf{U} = \mathbf{F} \Rightarrow \begin{bmatrix} -17.67 & -206.7 \\ -228.2 & -99.41 \end{bmatrix} \begin{bmatrix} u_1 \\ u_2 \end{bmatrix} = \begin{bmatrix} F_A \\ F_B \end{bmatrix} \tag{24}$$

Because no coupling exists between u_1 and u_2, modal variables η_1 and η_2 are solved independently, as in the IMSC approach. The rate indicator λ is undefined because this case is fully actuated.

The roots of the characteristic Eq. (21) in the form of Eq. (22) have the following real and imaginary parts:

$$\alpha_1 = 12.27 \qquad \alpha_2 = 14.83 \qquad \beta_1 = 55.19 \qquad \beta_2 = 66.69 \tag{25}$$

These parameters characterize the system dynamics. Vibrations with the first modal frequency $\beta_1 \approx \omega_1$ will be reduced to within 3% of their final values after $t_1^{3\%} = 0.2852$ s and those with the second modal frequency $\beta_2 \approx \omega_2$ after $t_2^{3\%} = 0.2360$ s. Figure 2a shows the actuation forces F_A and F_B that are required, Fig. 2b shows the tip deflections X_x^P (i.e., the deflection of point P in the x direction) and X_y^P as a function of time, and Fig. 2c shows the trajectory of point P as it appears in the xy plane, when viewed from the z direction. Because only the first two modes are considered in this case, any component of the disturbance affecting the third mode will be left unattenuated (the effect of this third mode is not shown in the plots of Fig. 2).

The effort indicator is $\kappa = 45 \cdot 10^3$, and the maximum attenuating forces are approximately 1450 N and 1250 N, for actuators F_A and F_B. Also, it appears that the action of force F_A is dominated by the frequency of the second mode, whereas the action of force F_B is predominately varying with the frequency of the first mode. This is consistent with Table 1, where member ***A*** contained a large fraction of strain energy for the second mode and member ***B*** contained a large fraction of the first mode's strain energy. The motion of the mast is approximately attenuated to 3% of the initial disturbance (2.28 mm in the x direction, 2.58 mm in the y direction) after just over two vibration cycles, or after tip point P orbits around its resting position just over two times.

Relocating the actuators will affect only the forces required to control two modes but not the trajectory shown in Fig. 2. For example, if such actuators are placed at locations ***D*** and ***E*** (see Fig. 1), then the effort indicator increases to $\kappa = 7826 \cdot 10^3$, and the maximum forces $F_D \approx 17,000$ N and $F_E \approx 14,500$ N will be required.

B. One Actuator, Replacing Member *A*, Controlling Two-Modes

Unlike fully actuated case 1, case 2 is underactuated, employing a single actuator in position ***A*** to attenuate the first two modes of

Table 1 Fraction of strain energy in selected members of the mast structure for first three modes of vibration

Member	Fraction of strain energy, mode 1, %	Fraction of strain energy, mode 2, %	Fraction of strain energy, mode 3,%
A	2.826	10.187	0.125
B	12.208	0.063	0.351
C	3.950	9.747	0.071

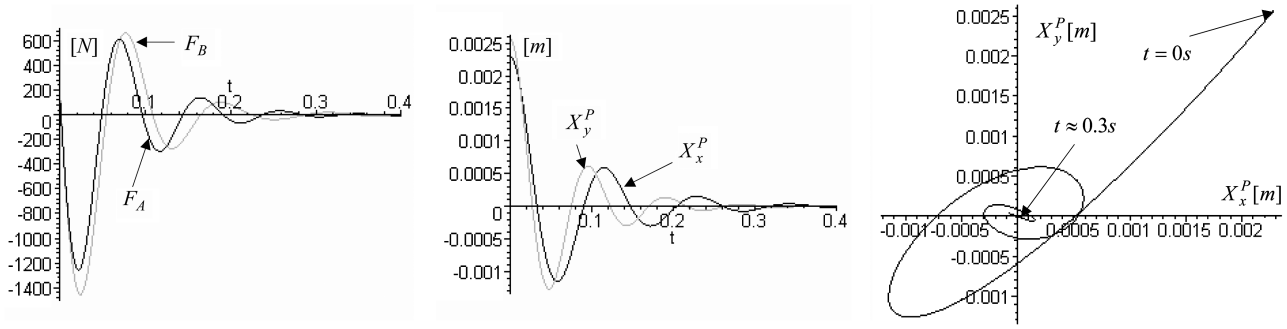

a) b) c)

Fig. 2 Graphs showing a) actuation forces F_A and F_B and tip deflections of point p X_x^p and X_y^p b) as a function of time, and c) as they appear in the xy plane.

vibration with the force F_A ($n_a = 1, n_m = 2, n_d = 1$). Therefore, the $n_d = 1$ constraint in the form of Eq. (18) is to be satisfied with the help of a Lagrange multiplier ensuring that only dynamically admissible trajectories are considered as solutions to the optimality Eq. (17).

The mapping between real actuation force F_A and dummy actuator force F_B, and modal controls u_1 and u_2 may be partitioned according to Eq. (6) as follows:

$$\hat{\mathbf{B}}^{-1}\mathbf{U} = \mathbf{F} \Rightarrow \begin{bmatrix} \tilde{\mathbf{B}}_\mathbf{a} & \tilde{\mathbf{B}}_\mathbf{r} \\ \mathbf{A}_\mathbf{a} & \mathbf{A}_\mathbf{r} \end{bmatrix} \begin{bmatrix} \mathbf{U}_\mathbf{a} \\ \mathbf{U}_\mathbf{r} \end{bmatrix} = \begin{bmatrix} \mathbf{F}_\mathbf{a} \\ \mathbf{F}_\mathbf{d} \end{bmatrix}$$
$$\Rightarrow \begin{bmatrix} -17.67 & -206.7 \\ -228.2 & -99.41 \end{bmatrix} \begin{bmatrix} u_1 \\ u_2 \end{bmatrix} = \begin{bmatrix} F_B \\ F_A \end{bmatrix} \tag{26}$$

Note that Eq. (26) is identical to Eq. (24) except that the former is partitioned such that u_1 is considered essential and u_2, redundant. In Eq. (29) all submatrices in $\hat{\mathbf{B}}^{-1}$ are single term scalars.

The constraint Eq. (7) is obtained from the lower partition of Eq. (26), which, when normalized according to Eq. (8), becomes independent of dummy actuator location, giving

$$\mathbf{A} = \begin{bmatrix} \mathbf{A}_\mathbf{a} & \mathbf{A}_\mathbf{r} \end{bmatrix} = \begin{bmatrix} 1 & 0.4357 \end{bmatrix} \tag{27}$$

By applying Eq. (9), the real attenuation force F_A is obtained in terms of the essential modal control u_1, as follows:

$$\mathbf{F}_\mathbf{a} = (\tilde{\mathbf{B}}_\mathbf{a} - \tilde{\mathbf{B}}_\mathbf{r}\mathbf{A}_\mathbf{r}^{-1}\mathbf{A}_\mathbf{a})\mathbf{U}_\mathbf{a} = \bar{\mathbf{B}}\mathbf{U}_\mathbf{a} \Rightarrow F_A = 456.8u_1 \tag{28}$$

The pseudotransfer matrix $\bar{\mathbf{B}}$ is represented by a scalar number in Eq. (28). It can be verified that it is independent of the dummy actuator location (i.e., F_B was chosen in this case, but F_C or F_D could have just as easily been chosen).

The rate indicator λ and effort indicator κ, defined in Eqs. (10a) and (10b), are obtained as follows:

$$\lambda = |\det \mathbf{A}_\mathbf{r}| = 0.4357 \qquad \kappa = |\det \bar{\mathbf{B}}| = 456.8 \tag{29}$$

Note the relationship between parameters in Eq. (29) and their relationship to the scalar terms in Eqs. (27) and (28). Recall that it is generally desirable to obtain λ close to unity and κ as small as possible. However, these rules are not precise correlations, particularly when comparing the values κ for cases with different dimensions (i.e., different numbers of actuators and/or modes).

The roots of the characteristic Eq. (21) take the complex form in Eq. (22), with the real and imaginary parts equal to

$$\alpha_1 = 3.785 \qquad \alpha_2 = 13.21 \qquad \beta_1 = 55.95 \qquad \beta_2 = 65.95 \tag{30}$$

The response parameters in Eq. (30) indicate that vibrations with the first mode frequency $\beta_1 \approx \omega_1$ approximately disappear after $t_1^{3\%} = 0.9247$ s and those with the second mode frequency $\beta_2 \approx \omega_2$ disappear after $t_2^{3\%} = 0.2650$ s. The fact that the first mode is dampened at a slower rate than the second is consistent with Table 1, which shows that the member $\boldsymbol{A}$ is better suited to attenuate the second mode than the first. Figure 3a shows the attenuation force F_A, and Figs. 3b and 3c show the tip deflections X_x^P and X_y^P.

The maximum force required over the control period is approximately 1150 N, somewhat smaller than the largest forces required in case 1. However, the attenuation of the first vibration mode takes about three times longer in case 2. From its disturbed state ($t = 0s$) the tip at P makes approximately six orbits about the resting position before the mast is effectively attenuated to 3% of the initial disturbance.

It is worth mentioning that if one actuator replacing member $\boldsymbol{B}$ is to control two modes then

$$\lambda = |\det \mathbf{A}_\mathbf{r}| = 11.70 \qquad \kappa = |\det \bar{\mathbf{B}}| = 219.7 \tag{31}$$

In comparison to case 2, λ becomes significantly larger than unity, indicating a slower attenuation rate of a particular mode. On the other hand κ has decreased, suggesting smaller magnitude attenuation forces.

The characteristic roots in Eq. (22), have the following real and imaginary parts:

$$\alpha_1 = 12.24 \qquad \alpha_2 = 0.7168 \qquad \beta_1 = 55.22 \qquad \beta_2 = 66.68 \tag{32}$$

These response parameters indicate that vibrations with the first modal frequency effectively disappear after $t_1^{3\%} = 0.2859$ s and those with the second modal frequency after $t_2^{3\%} = 4.883$ s. The second mode is attenuated much slower than in before for case 2. This is because member $\boldsymbol{B}$ contains only a small fraction of strain energy in the second mode (Table 1). In fact, member $\boldsymbol{B}$ approximately lies along the neutral bending plane of the mast under the bending deflections of the second mode. The maximum force required over the control period is approximately 1000 N, slightly smaller less than before, which is consistent with the reduction of κ.

However, if one actuator replacing member $\boldsymbol{C}$ is used then

$$\lambda = |\det \mathbf{A}_\mathbf{r}| = 0.5267 \qquad \kappa = |\det \bar{\mathbf{B}}| = 386.3 \tag{33}$$

The roots from Eq. (22) are

$$\alpha_1 = 4.514 \qquad \alpha_2 = 12.57 \qquad \beta_1 = 56.23 \qquad \beta_2 = 65.67 \tag{34}$$

Vibrations with the frequency of the first mode are effectively eliminated after $t_1^{3\%} = 0.7754$ s and those with the frequency of the second mode are attenuated after $t_2^{3\%} = 0.2784$ s, which is quicker than in case 2. This was expected because member $\boldsymbol{C}$ contains a larger fraction of strain energy in this mode (Table 1).

C. Two Actuators, Replacing Members *A* and *B*, Controlling Three Modes

Attenuating three modes of vibration with actuators in the locations of members $\boldsymbol{A}$ and $\boldsymbol{B}$ is an underactuated problem with

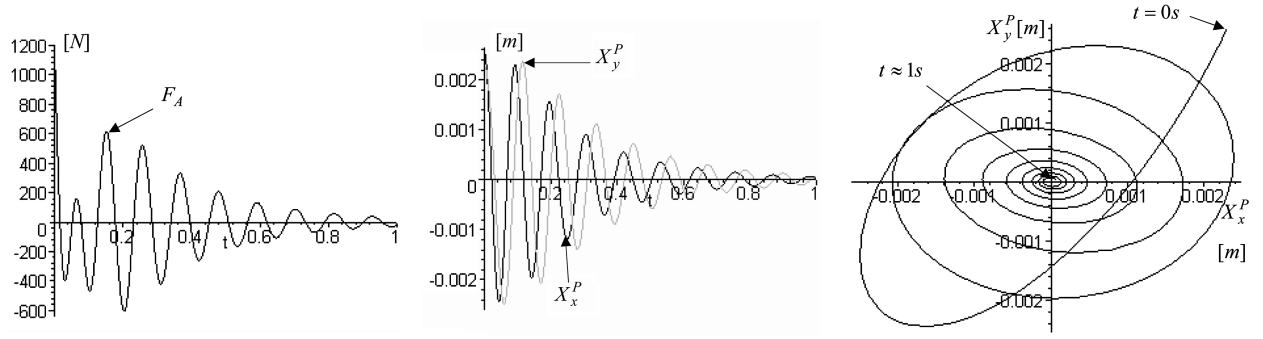

a) b) c)

Fig. 3 Graphs showing a) attenuation force F_A and tip deflections of point p X_x^p and X_y^p b) as functions of time, and c) as they appear in the xy plane.

$n_a = 2$, $n_m = 3$, $n_d = 1$. This actuator configuration is identical to case 1, however, forces F_A and F_B must also attenuate the mast's third twisting mode.

The mapping between real forces F_A and F_B and dummy force F_C, and modal controls u_1 and u_2, may be written according to Eq. (6) as follows:

$$\hat{\mathbf{B}}^{-1}\mathbf{U} = \mathbf{F} \Rightarrow \begin{bmatrix} \tilde{\mathbf{B}}_\mathbf{a} & \tilde{\mathbf{B}}_\mathbf{r} \\ \mathbf{A}_\mathbf{a} & \mathbf{A}_\mathbf{r} \end{bmatrix} \begin{bmatrix} \mathbf{U}_\mathbf{a} \\ \mathbf{U}_\mathbf{r} \end{bmatrix} = \begin{bmatrix} \mathbf{F}_\mathbf{a} \\ \mathbf{F}_\mathbf{d} \end{bmatrix}$$

$$\Rightarrow \begin{bmatrix} -21.84 & -210.6 & 2.976 \\ -223.9 & -95.46 & -3.050 \\ 137.2 & 126.7 & -97.84 \end{bmatrix} \begin{bmatrix} u_1 \\ u_2 \\ u_3 \end{bmatrix} = \begin{bmatrix} F_A \\ F_B \\ F_C \end{bmatrix} \tag{35}$$

By eliminating the dummy actuator ($F_C = 0$) the normalized constraint matrix as in Eq. (8) is obtained as follows:

$$\mathbf{A} = \begin{bmatrix} \mathbf{A}_\mathbf{a} & \mathbf{A}_\mathbf{r} \end{bmatrix} = \begin{bmatrix} 1 & 0.9237 & -0.7132 \end{bmatrix} \tag{36}$$

The real attenuation forces F_A and F_B are obtained in terms of the essential modal control u_1 and u_2 through Eq. (9) as shown in the following:

$$\mathbf{F}_\mathbf{a} = \bar{\mathbf{B}}\mathbf{U}_\mathbf{a} \Rightarrow \begin{bmatrix} F_A \\ F_B \end{bmatrix} = \begin{bmatrix} -17.67 & -206.7 \\ -228.2 & -99.41 \end{bmatrix} \begin{bmatrix} u_1 \\ u_2 \end{bmatrix} \tag{37}$$

The rate indicator λ and effort indicator κ are

$$\lambda = |\det \mathbf{A}_\mathbf{r}| = 0.7132 \qquad \kappa = |\det \bar{\mathbf{B}}| = 45.41 \cdot 10^3 \tag{38}$$

In comparison to case 2, λ is now closer to unity indicating that a faster rate of attenuation should be expected. Also, κ is identical to case 1, as both of these cases (i.e., 1 and 3) use the same actuator configuration. The roots in Eq. (22) have the following real and imaginary parts:

$$\alpha_1 = 12.06 \qquad \alpha_2 = 14.51 \qquad \alpha_3 = 24.99$$
$$\beta_1 = 55.20 \qquad \beta_2 = 66.69 \qquad \beta_3 = 425.7 \tag{39}$$

Vibrations with the frequency of the first mode $\beta_1 \approx \omega_1$ effectively disappear after $t_1^{3\%} = 0.2902$ s, those with the frequency of the second mode $\beta_2 \approx \omega_2$ after $t_2^{3\%} = 0.2412$ s, and those with the frequency of the third mode $\beta_3 \approx \omega_3$ after $t_3^{3\%} = 0.1401$ s. By comparing the dynamic response parameters in Eq. (39) to those of case 1 [see Eq. (25)] it is evident that the first two modes are attenuated with very similar rates and frequencies, despite the fact that the third mode is also attenuated by the actions of F_A and F_B. The attenuation forces F_A and F_B are shown in Fig. 4a, the tip deflections X_x^P and X_y^P are shown in Figs. 4b and 4c, and the tip rotation X_{rotz}^P is shown inset in Fig. 4b.

The maximum forces required over the control period are approximately 2400 N and 2800 N for actuation forces F_A and F_B, respectively. Note how the end deflections of point p are hardly affected by the third twisting mode, as the tip deflections shown in Figs. 4b and 4c are nearly identical to case 1, where the third mode was neglected. However, the tip rotation clearly shows the relatively quick attenuation of this mode. Like in case 1, the mast's tip orbits about the resting position a little over two times before the disturbance is effectively attenuated to 3% of its initial value.

D. One Actuator, Replacing Member *A*, Controlling Three Modes

This final underactuated case uses a single actuator in the location of member ***A*** to attenuate the mast's first three vibration modes ($n_a = 1$, $n_m = 3$, $n_d = 2$). Though the actuator configuration is identical to case 2, force F_A is to attenuate also the third mode of vibrations.

The mapping between the real force F_A and dummy forces F_B and F_C, and modal controls u_1, u_2, and u_3, may be written according to Eq. (6) as follows:

$$\hat{\mathbf{B}}^{-1}\mathbf{U} = \mathbf{F} \Rightarrow \begin{bmatrix} \tilde{\mathbf{B}}_\mathbf{a} & \tilde{\mathbf{B}}_\mathbf{r} \\ \mathbf{A}_\mathbf{a} & \mathbf{A}_\mathbf{r} \end{bmatrix} \begin{bmatrix} \mathbf{U}_\mathbf{a} \\ \mathbf{U}_\mathbf{r} \end{bmatrix} = \begin{bmatrix} \mathbf{F}_\mathbf{a} \\ \mathbf{F}_\mathbf{d} \end{bmatrix}$$

$$\Rightarrow \begin{bmatrix} -21.84 & -210.6 & 2.976 \\ -223.9 & -95.46 & -3.050 \\ 137.2 & 126.7 & -97.84 \end{bmatrix} \begin{bmatrix} u_1 \\ u_2 \\ u_3 \end{bmatrix} = \begin{bmatrix} F_A \\ F_B \\ F_C \end{bmatrix} \tag{40}$$

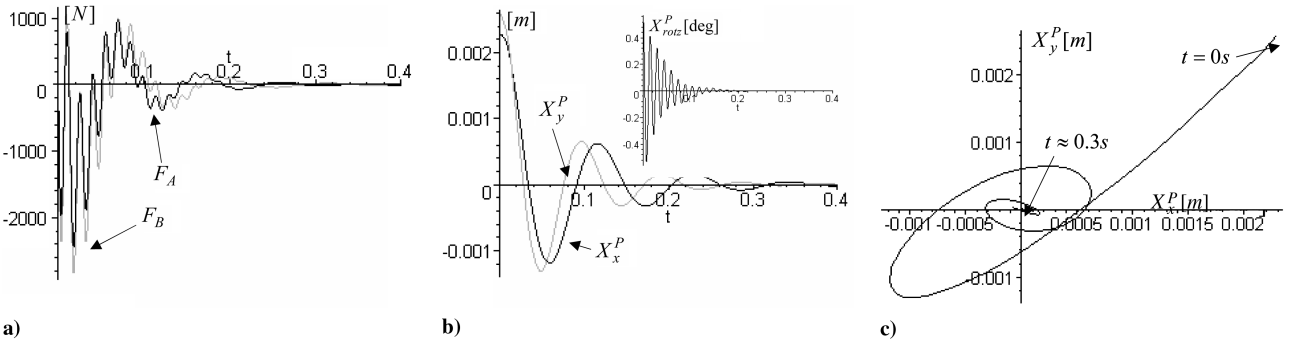

a) b) c)

Fig. 4 Graphs showing a) attenuation forces F_A and F_B, tip deflections of point p X_x^p and X_y^p b) as functions of time, and c) as they appear in the xy plane, and (b inset) rotation of point p X_{rotz}^p as a function of time.

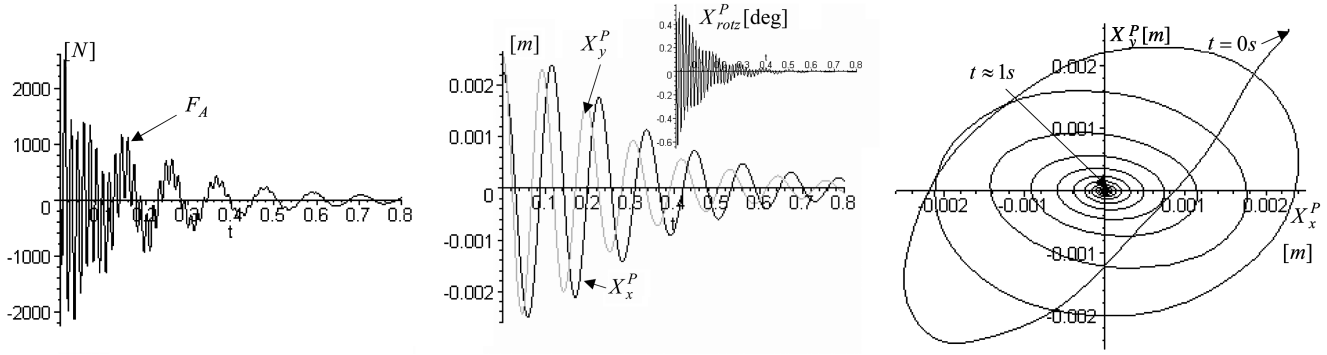

a) b) c)

Fig. 5 a) Attenuation force F_A, tip deflections of point p X_x^P and X_y^P b) as functions of time, and c) as they appear in the xy plane, and (b-inset) rotation of point p X_{rotz}^P as a function of time.

Note that this equation is identical to Eq. (35) (for case 3), only that the arrangement of the partition has been modified to suit the new dimensions of case 4.

Upon eliminating the dummy actuators ($F_B = F_C = 0$) the normalized constraint matrix in the form of Eq. (8) is obtained as

$$\mathbf{A} = \begin{bmatrix} \mathbf{A_a} & \mathbf{A_r} \end{bmatrix} = \begin{bmatrix} 1 & 0.4357 & 0 \\ 0 & 1 & -1.462 \end{bmatrix} \tag{41}$$

The real attenuation force F_A may be obtained in terms of the essential modal control u_1 through Eq. (9), as shown in the following:

$$\mathbf{F_a} = \bar{\mathbf{B}}\mathbf{U_a} \Rightarrow F_A = 456.8u_1 \tag{42}$$

The rate indicator λ and effort indicator κ are

$$\lambda = |\det \mathbf{A_r}| = 0.6370 \qquad \kappa = |\det \bar{\mathbf{B}}| = 456.8 \tag{43}$$

In comparison to case 2, the preceding λ is closer to unity, indicating that a faster rate of attenuation should be expected. Also, as expected, κ is identical to case 2, as both cases use the same actuator configuration.

The characteristic roots, in the complex form of Eq. (22), have the following real and imaginary parts:

$$\alpha_1 = 3.779 \qquad \alpha_2 = 13.14 \qquad \alpha_3 = 8.980$$
$$\beta_1 = 55.95 \qquad \beta_2 = 65.96 \qquad \beta_3 = 425.7 \tag{44}$$

Vibrations with the frequency $\beta_1 \approx \omega_1$ are effectively attenuated after $t_1^{3\%} = 0.9262$ s, those with the second frequency $\beta_2 \approx \omega_2$ after $t_2^{3\%} = 0.2664$ s, and those with the frequency $\beta_3 \approx \omega_3$ are eliminated after $t_3^{3\%} = 0.3898$ s. When comparing the response parameters in Eq. (44) to those of case 2 [see Eq. (30)], it is evident that the first two modes are attenuated with very similar rates and frequencies, despite the fact that the third mode is also attenuated by the action of force F_A. The attenuation force F_A is shown in Fig. 5a, the tip deflections X_x^P and X_y^P are shown in Figs. 5b and 5c, and the tip rotation X_{rotz}^P is shown inset in Fig. 5b.

The maximum actuation force F_A over the control period is approximately 2400 N. As in case 3, the end deflections of point p are hardly affected by the third twisting mode and therefore the deflected tip response shown in Figs. 5b and 5c is nearly identical to case 2. The third mode, visible in the plot of the rotation of point p, is attenuated quite quickly (less than 0.4 s) in comparison to the more persistent first bending mode. The disturbance is attenuated to 3% after the tip orbits about the resting position approximately eight times.

IV. Conclusions

A procedure for analyzing and simulating active optimal vibration control of underactuated elastic structural systems is presented. Underactuated systems must obey additional constraints imposed on possible motions. These constraints are nonintegrable (nonholonomic) in terms of the modal variables (or the system's degrees of freedom) but algebraic (holonomic) in terms of the modal controls. The algebraic form of the constraints can be used to formulate the normalized constraint matrix and the pseudotransfer matrix. These two matrixes, which are determined in the early phase of the analysis, depend only on the placement of the actuators, and therefore define the system's controllability. The attenuation rate and effort parameters can be used to compare controllability of a system with different configurations of actuators.

The procedure combines the use of the FE and symbolic mathematics standard software to analyze and simulate the entire control process, including the actuation and the response histograms. As the examples demonstrate, a poor placement of actuators leading to an excessively long attenuation time of a particular mode is indicated by large numerical values of some coefficients of the constraint matrix or a large value of the rate parameter. In turn, large values of coefficients in the pseudotransfer matrix or a large value of the effort parameter signal excessively large actuation forces. The preceding properties of the constraint and pseudotransfer matrices may be used for a preliminary assessment of the actuation setup, which can be done within the problem's structural phase (and using only the FE software), without actually entering the control phase (i.e., without using the symbolic operations that require the mathematical software). A verification phase may also be performed to investigate any spillover effects on higher vibration modes that were not considered in the control phase.

References

[1] Fantoni, I., and Lozano, R., *Non-Linear Control for Underactuated Mechanical Systems*, Springer–Verlag, New York, 2002, Chaps. 1, 2.

[2] Bathe, K. J., *Finite Elements Procedures*, Prentice–Hall, Upper Saddle River, NJ, 1996, Chap. 9.3.

[3] Calfield, R. A., and Meirovitch, L., "Integrated Structural Design and Vibration Suppression Using Independent Modal Space Control," *AIAA Journal*, Vol. 32, No. 10, 1994, pp. 2053–2060. doi:10.2514/3.12251

[4] Szyszkowski, W., and Dhotre, N., "A Procedure for Solving Under-Actuated Optimal Attenuation of Vibrations by Means of Symbolic Operators," *Journal of Vibration and Control* (to be published).

[5] Woods, S., and Szyszkowski, W., "Analysis and Simulation of Optimal Vibration Attenuation for Under-Actuated Mechanical Systems," *AIAA Journal* (submitted for publication).

[6] Kirk, D. E., *Optimal Control Theory*, Dover, New York, 1998, Chap. 5.

[7] Zill, D. G., and Cullen, M. R., *Advanced Engineering Mathematics*, PWS Publishing, Boston, MA, 1992, Chap. 5.

[8] Szyszkowski, W., and Baweja, M., "The FEM Optimization of Active Vibration Control in Structures by Solving the Corresponding Two-Point-Boundary-Value Problem," *Structural and Multidisciplinary Optimization*, Vol. 34, No. 6, 2007, pp. 525–537.

[9] Preumont, A., *Vibration Control of Active Structures: An Introduction*, 2nd ed., Kluwer Academic, Norwell, MA, 2002, Chaps. 3, 13.